Relative stability of low-index V_2O_5 surfaces: a density functional investigation

2009 J. Phys.: Condens. Matter 21 095008

(http://iopscience.iop.org/0953-8984/21/9/095008)

J. Phys.: Condens. Matter **21** (2009) 095008 (8pp) doi:10.1088/0953-8984/21/9/095008

Relative stability of low-index V_2O_5 surfaces: a density functional investigation

Jakub Goclon[1], Robert Grybos[1,2,3], Małgorzata Witko[1] and Jürgen Hafner[2]

[1] Institute of Catalysis and Surface Chemistry PAS, Krakow, Poland
[2] Fakultät für Physik and Center for Computational Material Science, Universität Wien, Vienna, Austria

E-mail: ncgrybos@cyf-kr.edu.pl

Received 4 December 2008, in final form 21 January 2009
Published 13 February 2009
Online at stacks.iop.org/JPhysCM/21/095008

Abstract

Ab initio density functional calculations of the structural and electronic properties of V_2O_5 bulk and its low-index surfaces are presented. For the bulk oxide and the (010) surface (the natural cleavage plane) a good agreement with experiment and with earlier *ab initio* calculations is found. For the first time, the investigations are extended to other low-index surfaces: (001) and (100). On both surfaces, termination conserving a bulk-like stoichiometry is preferred, but—in contrast to the (010) surface—a strong structural relaxation takes place. Relaxation reduces the surface energy from 1.16 to 0.48 J m^{-2} for the (001) and from 0.61 to 0.55 J m^{-2} for the (100) surface. Although the relaxed surface energies are still one order of magnitude higher than calculated for the (010) surface (0.047 J m^{-2}), the Wulff construction demonstrates that (001) and (100) surfaces contribute about 15% of the total surface area of a V_2O_5 crystallite, indicating a non-negligible role in the catalytic activity of V_2O_5.

1. Introduction

Vanadia-based catalysts are used for many industrial processes such as selective oxidation of hydrocarbons and sulfur dioxide, oxidative dehydrogenation of hydrocarbons and selective catalytic reduction (SCR) of nitric oxide by ammonia [1–3]. According to the oxidation mechanism proposed by Mars and van Krevelen [4], oxygen from the catalyst surface is transferred to the adsorbed molecule, leaving a vacancy behind. Afterwards the catalyst surface undergoes re-oxidation by gas-phase oxygen. Therefore the catalyst activity directly depends on the ease of creation of oxygen vacancies.

Catalysts based on transition metal oxides often exhibit a pronounced crystallographic anisotropy, as different surfaces expose different types of active sites, which participate in different elementary steps of catalytic reaction. In particular, the presence or absence of coordinatively unsaturated surface sites strongly affects the adsorption/activation of hydrocarbon molecules.

Despite the great importance of V_2O_5 many details of its catalytic behaviour are still not sufficiently understood. Theoretical studies of the electronic structure were performed using both cluster [5–8] and periodic [9–12] models and concentrated on the (010) surface due to the fact that only the (010) surface was observed in scanning tunnelling microscopy (STM) [13–16] and atomic force microscopy (AFM) [16, 17]. It was postulated that on naturally grown crystallites only minor fractions of other surfaces are exposed and the catalytic processes necessarily take place on the most stable V_2O_5(010) surface. However, there are no *a priori* indications that the activity of other surfaces like (001) or (100) should be excluded. To the best of our knowledge, surfaces other than (010) were not studied so far, neither theoretically nor experimentally.

In this paper, periodic DFT calculations for bulk V_2O_5 and for three defect-free low-index surfaces: (010), (001) and (100), the last one with different surface terminations, are reported. Statistical thermodynamics is used to study the stability of four possible terminations of the (100) V_2O_5 surface as a function of temperature and partial pressure of oxygen in the gas phase. Wulff construction is used to determine the approximate equilibrium crystallite morphology of V_2O_5. The electronic structure of different surfaces is represented by their atom-projected partial densities of states (DOS). The DOS for the (010)

[3] Author to whom any correspondence should be addressed.

surface is compared with available angle-resolved ultraviolet photoemission spectroscopy (ARUPS) data [18].

This paper is organized as follows: after description of the computational methodology in section 2, section 3 provides a short characterization of the crystal structure of V_2O_5 and of the geometry of the three low-indices surfaces. Results for the atomic and electronic structures of the relaxed surfaces are presented and discussed in section 4, whereas section 5 summarizes the most important findings.

2. Methodology

2.1. Computational details

Periodic *ab initio* DFT calculations were performed using the Vienna *ab initio* simulation package (VASP) [25, 19] with the gradient corrected functional PW91 [22, 20]. The calculations were carried out in a plane-wave basis set, using the projector-augmented wave method (PAW) [24, 21], as implemented by Kresse and Joubert [25, 19], to describe the electron–ion interaction. The 3p states of V were treated as valence states to guarantee a good transferability of the V pseudopotential and for O both the 2s and 2p states were included in the valence region. The energy cutoff was set to 600 eV.

Surfaces were simulated by slabs separated by a sufficiently wide vacuum region (10–15 Å). The number of k-points for Brillouin-zone integration (BZ) was chosen according to the Monkhorst–Pack [22] scheme. For bulk V_2O_5 a $2 \times 6 \times 2$ grid was used, whereas for the supercells representing (010), (001) and (100) surfaces $2\times1\times6$, $2\times6\times1$ and $1 \times 6 \times 6$ grids were applied, respectively, allowing an accuracy of the Brillouin-zone integrations of better than 1 meV per atom. Positions of all atoms were relaxed using a conjugate-gradient algorithm. The surface energy E_{surf} was calculated as the difference between the total energy of the slab and the total energy of an equal number of V_2O_5 units in the bulk, divided by the surface area A (on both sides of the slab), $E_{\mathrm{surf}} = (E^{\mathrm{DFT}}_{\mathrm{slab}} - E^{\mathrm{DFT}}_{\mathrm{bulk}})/2A$.

2.2. Thermodynamic analysis

The thermodynamic formalism used to determine the most stable termination of the (100) V_2O_5 surface at a given temperature and O_2 partial pressure is described in detail in [23]. It is considered a surface in contact with an oxygen atmosphere with partial pressure p and temperature T and assumed that the environment acts as a reservoir and can exchange any amount of oxygen with the sample without changing its temperature or pressure. The appropriate thermodynamic potential required to describe such a system is the Gibbs free energy that also depends on the number of vanadium (N_{V}) and oxygen (N_{O}) atoms in the sample. The most stable surface composition and geometry is then the one that minimizes the surface free energy $\gamma(T, p)$ defined as

$$\gamma(T,p) = \frac{1}{A}[G(T,p,N_{\mathrm{V}},N_{\mathrm{O}}) - N_{\mathrm{V}}\mu_{\mathrm{V}}(T,p) - N_{\mathrm{O}}\mu_{\mathrm{O}}(T,p)] \quad (1)$$

where $\mu_{\mathrm{V}}(T, p)$ and $\mu_{\mathrm{O}}(T, p)$ are the chemical potentials of V and O atoms, respectively. The chemical potentials of vanadium and oxygen are, in fact, not independent; thermodynamic equilibrium with bulk V_2O_5 requires that

$$4\mu_{\mathrm{V}}(T,p) + 10\mu_{\mathrm{O}}(T,p) = g^{\mathrm{bulk}}_{V_2O_5}(T,p) \quad (2)$$

where $g^{\mathrm{bulk}}_{V_2O_5}(T, p)$ is the Gibbs free energy per V_2O_5 elementary cell containing two formula units. Inserting this constraint into equation (1) leads to

$$\gamma(T,p) = \frac{1}{A}\Big[G(T,p,N_{\mathrm{V}},N_{\mathrm{O}}) - \frac{N_{\mathrm{V}}}{4}g^{\mathrm{bulk}}_{V_2O_5}(T,p) + \big(\tfrac{10}{4}N_{\mathrm{V}} - N_{\mathrm{O}}\big)\mu_{\mathrm{O}}(T,p)\Big]. \quad (3)$$

Here $G(T, p, N_{\mathrm{V}}, N_{\mathrm{O}})$ is the Gibbs free energy of a slab representing the surface and A is the area of the slab surface in the unit cell. Neglecting atomic vibrations, the Gibbs free energy may be approximated by the internal energy, which is determined by DFT total-energy calculations, so finally

$$\gamma(T,p) = \frac{1}{A}\Big[E^{\mathrm{DFT}}_{\mathrm{slab}} - \frac{N_{\mathrm{V}}}{4}E^{\mathrm{DFT}}_{\mathrm{bulk}} + \big(\tfrac{10}{4}N_{\mathrm{V}} - N_{\mathrm{O}}\big)\mu_{\mathrm{O}}(T,p)\Big]. \quad (4)$$

Calculating the vibrational contribution to the Gibbs free energy involves determining accurate phonon densities, which is very time-consuming. Reuter and Sheffler [23] have estimated this contribution for ruthenium oxide using the Einstein model and obtained a value below 10 meV. Such a modest change in surface energy does not influence our discussion and conclusions. It is important to consider the upper and lower limit of $\mu_{\mathrm{O}}(T, p)$. If $\mu_{\mathrm{O}}(T, p)$ is too low, V_2O_5 is reduced to a lower-valence oxide (for example, to VO_2). This imposes a lower limit on the oxygen chemical potential $\mu_{\mathrm{O}}(T, p)$ defined by

$$\mu^{\mathrm{min}}_{\mathrm{O}}(T,p) \leqslant \tfrac{1}{2}[E^{\mathrm{bulk}}_{V_2O_5} - 2E^{\mathrm{bulk}}_{VO_2}], \quad (5)$$

where $E^{\mathrm{bulk}}_{V_2O_5}$ and $E^{\mathrm{bulk}}_{VO_2}$ are the DFT total energies per unit cell for bulk V_2O_5 and VO_2, respectively. On the other hand, for very high pressures, molecular oxygen starts to condense on the surface. Thus the upper limit of the oxygen chemical potential is given by

$$\mu^{\mathrm{max}}_{\mathrm{O}}(T,p) = \tfrac{1}{2}E^{\mathrm{DFT}}(\mathrm{O}_2). \quad (6)$$

Therefore, the variation of the oxygen chemical potential $\mu_{\mathrm{O}}(T, p)$ is limited to the interval

$$\tfrac{1}{2}[E^{\mathrm{bulk}}_{V_2O_5} - 2E^{\mathrm{bulk}}_{VO_2}] < \mu_{\mathrm{O}}(T,p) < \tfrac{1}{2}E^{\mathrm{DFT}}(\mathrm{O}_2). \quad (7)$$

2.3. Wulff construction

Knowing the energies of different surfaces, it is possible to predict the equilibrium morphology of vanadia crystallites using the Wulff method [24]. In this construction, the distances d_{hkl} of (hkl) facets from the crystal's centre are proportional to their surface energies. The most stable surfaces have the lowest d_{hkl} values and thus dominate the overall shape of the crystallite according to the relation

$$\frac{E_{\mathrm{surf}}(ijk)}{E_{\mathrm{surf}}(lmn)} = \frac{d_{ijk}}{d_{lmn}}. \quad (8)$$

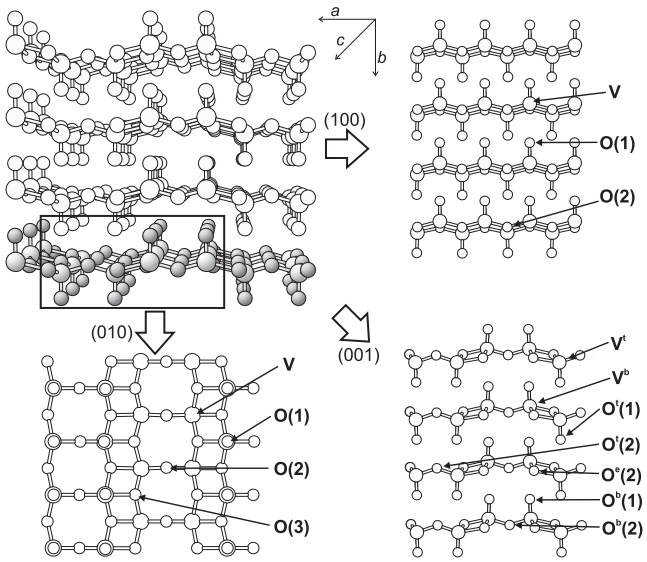

Figure 1. View of the V_2O_5 bulk structure (with unit cell indicated) and three low-index surfaces (in top view). Different types of oxygen and vanadium centres are shown.

Table 1. Lattice constants (in Å) and internal positions of atom centres inside the optimized and crystallographic cell of bulk V_2O_5. Experimental values [25] are given in parentheses. (Note: position (4f): x, 1/4, z; $-x+1/2$, 1/4, z; $-x$, 3/4, $-z$; $x+1/2$, 3/4, $-z$. Position (2a): 1/4, 1/4, z; 3/4, 3/4, $-z$.)

	a	*b*	*c*
Lattice (Å)	11.65 (11.51)	4.66 (4.37)	3.57 (3.56)
Atom	*x*	*y*	*z*
V in (4f)	0.10 (0.10)	0.89 (0.89)	1/4 (1/4)
O(1) in (4f)	0.11 (0.10)	0.55 (0.53)	1/4 (1/4)
O(2) in (2a)	0.25 (1/4)	0.00 (0.00)	1/4 (1/4)
O(3) in (4f)	−0.07(−0.07)	0.00 (0.00)	1/4 (1/4)

Our analysis was restricted to the three low-indices surfaces and therefore may not represent the actual shape of a real crystallite. It reflects only the relative energies of the studied V_2O_5 surfaces and their contribution to the overall surface area of a crystallite.

3. Structural and electronic properties of bulk V_2O_5

3.1. Crystal structure of V_2O_5

V_2O_5 has a layer-type structure and crystallizes in an orthorhombic lattice (space group D_{2h}-P_{mmn}), which may be viewed as a stacking of closely packed, but weakly interacting, saturated layers (dubbed s-layers) along the [010] direction (see figure 1). In the present studies the orientation of the crystallographic axes given in the original reference on the crystal structure [25] was adopted, with s-layers stacking along the b direction, although in the literature b and c axes are sometimes interchanged. The lattice parameters are $a = 11.512$ Å, $b = 4.364$ Å and $c = 3.564$ Å [25, 26]. The elementary unit cell contains 14 atoms (2 stoichiometric units).

Vanadyl oxygen atoms O(1) (in Wyckoff position (4f)) are bound by a double bond (along the c direction) to V with distance equal to 1.58 Å. The bridging oxygen atoms O(2) (in Wyckoff position (2a)) connect along the a direction two V atoms with equal bond distances of 1.78 Å. Threefold-coordinated oxygen atoms O(3) (in Wyckoff positions 4(f)) have two shorter (1.88 Å) and one longer (2.02 Å) bonds along the c and a directions, respectively.

Vanadium is coordinated to five oxygen atoms (one O(1), two O(2) and three O(3)) within the same s-layer; in addition, there is a weak bond to vanadyl oxygen from the neighbouring s-layer with a length of 2.78 Å. The structure is usually represented by edge-and corner-sharing square pyramids, where pyramids sharing an edge have opposite orientation in the b direction, whereas corner-sharing pyramids have the same orientation.

The optimization of unit cell shape and of the internal atomic coordinates was performed for 21 fixed volumes. The equilibrium volume was obtained by fitting the calculated total energies to a Murnaghan [27] equation of state. For the resulting optimal volume, cell vectors were carefully optimized to find the optimal cell shape. Obtained unit vectors are $a = 11.65$ Å, $b = 4.66$ Å and $c = 3.57$ Å. These values compare well with the experimental data cited above and are within the range obtained through other calculations—see tables 1 and 2. Note that our cell shape differs slightly from the one obtained by Ganduglia-Pirovano *et al* [11]. The relative error (compared to experiment) is largest (6.6%) for the lattice vector b, perpendicular to the s-layers, indicating a non-negligible van der Waals contribution to inter-layer cohesion. The computed intra-layer V–O bond lengths (table 3) $d_{V-O(1)} = 1.61$ Å, $d_{V-O(2)} = 1.79$ Å, $d_{V-O(3)} = 1.89$ Å and $d_{V-O(3)} = 2.05$ Å, match very well the corresponding experimental values (1.58, 1.78, 1.88 and 2.02 Å, respectively). The length of the inter-layer van der Waals bond is 3.06 Å, larger by 0.27 Å than given by experiment. The discrepancy between calculated and experimental lengths of the lattice vector b is 0.29 Å, which strongly suggests that the lattice vector overestimation arises solely from the insufficient description of van der Waals forces. Similar observations apply to other layer-type materials such as graphite, BN and MoS_2. Currently, new exchange–correlation functionals with an improved treatment of dispersion forces

Table 2. Experimental and optimized lattice constants obtained in the present work and from other DFT (GGA) calculations. Axes b and c in the original papers may be interchanged.

References	*a* (Å)	*b* (Å)	*c* (Å)
Experiment [25]	11.51	4.37	3.56
VASP This work	**11.65**	**4.66**	**3.57**
VASP (Kresse *et al*) [10]	11.65	4.69	3.57
VASP (GP *et al*) [11]	11.55	4.84	3.58
CPMD (GP *et al*) [12]	11.62	4.44	3.59

Table 3. Calculated V–O bond distances (in Å) for the V_2O_5 bulk and (010) surface, compared to experiment (after [25]).

O(x)–V bond	Bulk (expt.)	Bulk (calc.)	(010) Surface (calc.)
O(1)–V	1.58	1.61	1.61
O(2)–V	1.78	1.79	1.81
O(3)–V	1.89, 2.02	1.89, 2.05	1.90, 2.06

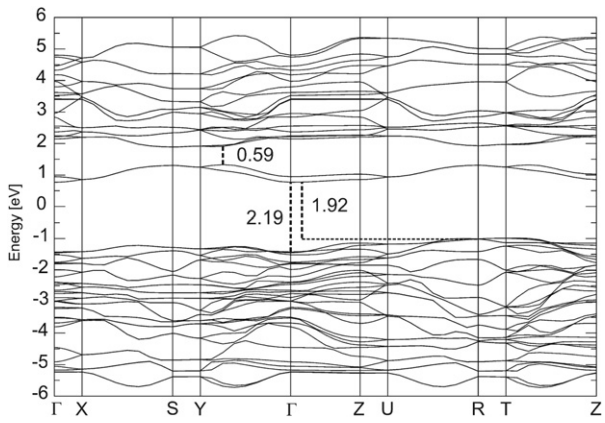

Figure 2. Electronic band structure of bulk V_2O_5. The bands are plotted along a path connecting high-symmetry points in the irreducible Brillouin zone. The Fermi energy defines the energy zero.

are in a test stage [28, 29], but these are computationally too demanding to be applied to large unit cells. In any case, the overestimation of the inter-layer distances in bulk V_2O_5 should not influence the description of low-index surfaces.

3.2. Electronic structure of bulk V_2O_5

Figure 2 shows the calculated electronic states along a selected path within the first Brillouin zone of the simple orthorhombic lattice.

The top of the valence band (VB) is located along the R–T direction while the bottom of the conduction band (CB) is at the Γ point. The calculated direct bandgap at Γ is 2.19 eV, which is slightly lower than the bandgap obtained from either photodesorption measurements (2.35 eV) [30], from optical adsorption (2.30 eV) [31] or from optical reflectance data (2.38 eV) [32]. The most characteristic feature of the band structure is splitting of the CB into two bands (see figure 2): a narrow and a much wider CB band that are separated from each other by a small gap of 0.59 eV. This splitting was already discussed in the literature [33, 34]. Results of calculations confirmed the character of V_2O_5 bulk as a semiconductor with an indirect bandgap of about 1.92 eV.

The total density of states (DOS) of bulk V_2O_5 is shown in figure 3(a). The width of the V_2O_5 bulk valence band (VB) is about 5.5 eV and DOS consists of three bands denoted as A, B and C. The VB is characterized as a mixture of O 2p and V 3d orbitals, where states originating from the O 2p dominate in peak A at the upper edge of the VB, while the contribution from V 3d is largest for peak C at the bottom of the VB. Peak B located at the VB centre arises from the V–O hybridization. In contrast, the conduction band is mainly composed of V 3d orbitals with a negligible contribution of O 2p states.

Experimental information is available from the x-ray photoemission (XPS) spectra of Shin *et al* [35] showing only a broad, rather symmetric band, approximately 6 eV wide. On the other hand, ultraviolet photoemission spectra (UPS) give a three-peak structure with a shoulder at high binding energies; relative intensity of peaks varies strongly with the

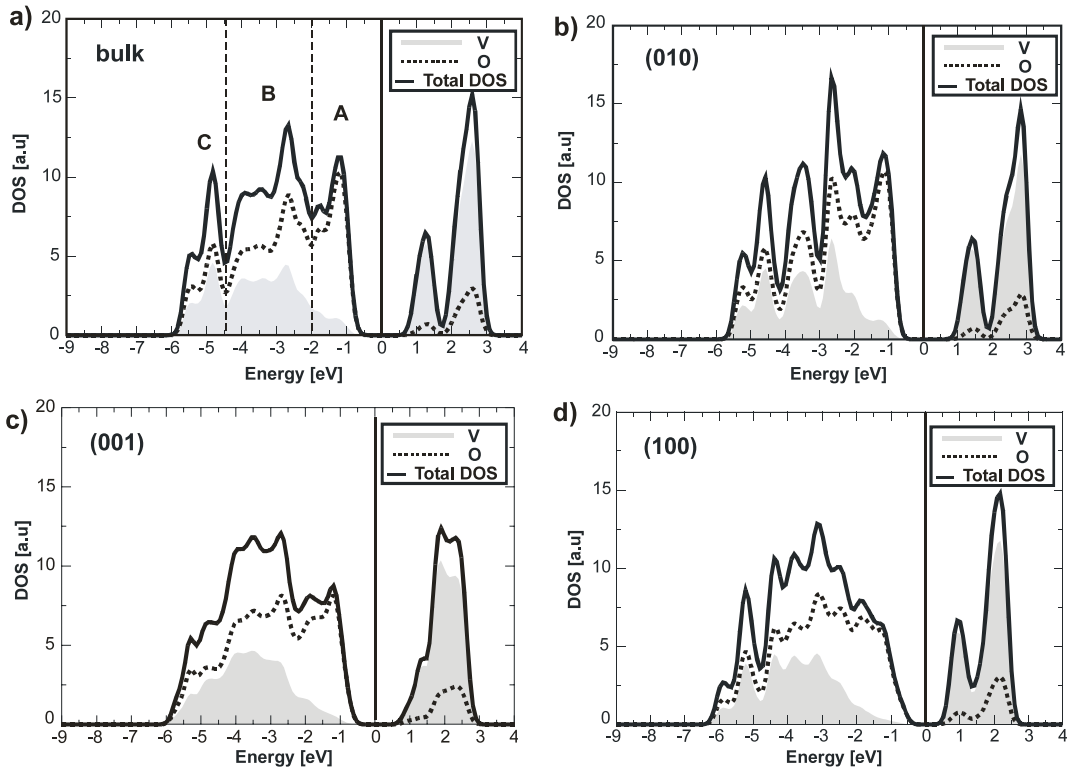

Figure 3. Total and partial electronic densities of states (DOS) of V_2O_5. Three peaks labelled A, B and C correspond to the peak in the photoemission spectra measured by Shin *et al* [35]. Parts (b)–(d) show the electronic DOS calculated for the (010), (001) and (d) (100)-t_1 V_2O_5 surfaces, respectively. The full line shows the total DOS, the dotted line the partial oxygen DOS and the shaded area the partial vanadium DOS. In all figures a Gaussian broadening of 0.2 eV is applied. The Fermi level is marked by a thin vertical line.

energy of the incident photons. The photoionization cross sections tabulated by Yeh and Lindau [36] show that the O 2p cross section decreases with the photon energy from 70 to 25 eV, while the V 3d cross section exposes a resonant increase at photon energies corresponding to the excitation of the V 3p semi-core states. Recently, resonant photoemission spectroscopy (RPES) with photon energies varying between 39 and 60 eV was also used by Wu *et al* [37] to explore the valence band structure of V_2O_5. From the observed variation of the UPS with the photon energy and from the RPES data it was concluded that the low-energy peak of the spectrum can be assigned to a non-bonding O 2p band, while the high-energy shoulder (consisting of two peaks) to band with an appreciable contribution of a V 3d component. Such an assignment agrees very well with our interpretation of the calculated partial DOS. However, even if the partial DOS are weighted with the relevant photoionization cross sections [36], the agreement between theory and experiment is only partial, as was shown in [38].

Another measurements by Khyzhun *et al* [39] using resonant soft x-ray emission gave spectra for a series of excitation energies at the V Kα and O Kα bands and showed that the V Lα spectrum consists of two distinct components assigned to the V $3e_g$ states hybridized with the O p_σ states and to the V $3t_{2g}$ states mixed with the O $2p_\pi$ states, the former feature appearing at higher binding energies due to the larger V $3e_g$–O $2p_\sigma$ overlap. Again this is in good agreement with our analysis of the partial DOS.

Good correspondence of our results with experimental data shows that the adopted computational set-up and the choice of functional are appropriate.

4. Geometric and electronic structure of the low-index surfaces of V_2O_5

4.1. Geometric structure of the V_2O_5 (010) surface

On the (010) surface five distinct oxygen sites are present (see figure 1): terminal oxygen atoms O(1) located above the vanadium atoms and bridging oxygen atoms, O(2), O′(2) linking two vanadyl groups and O(3), O′(3) linking three vanadyl groups. The primed sites O′(2) and O′(3) are not easily accessible from above the surface and will not be further considered. Atoms on the (010) surface are coordinatively saturated; hence the interaction between the layers is mainly of the van der Waals type.

Because of the weak interaction between adjacent crystal layers the structure of the (010) surface of V_2O_5 is sufficiently well described by only one isolated s-layer, using a single elementary cell (containing 14 atoms) as a supercell. Indeed, the surface relaxations are very small and the atom positions differ only slightly from the bulk (see table 3). The $d_{V-O(1)}$ distances are the same as in the bulk whereas the $d_{V-O(2)}$, $d_{V-O'(2)}$, $d_{V-O(3)}$ and $d_{V-O'(3)}$ bond lengths are larger only by 0.02, 0.02, 0.01 and 0.01 Å, respectively. These results are in agreement with the calculations of Ganduglia-Pirovano [11]. To check the accuracy of the results based on this 'single-layer supercell', additional calculations were performed for a two-layer model, yielding differences between the V–O bond lengths in both models no bigger than 0.03 Å. Since cleavage along the (010) plane requires only the breaking of van der Waals bonds, the surface energy of the V_2O_5(010) surface is very low even for an unrelaxed, bulk-terminated geometry ($E_{surf} = 0.054$ J m^{-2}). If a full relaxation is allowed, this value is only slightly reduced to 0.047 J m^{-2}.

4.2. Geometric structure of the V_2O_5 (001) surface

The V_2O_5 (001) surface is more corrugated, consisting of alternating 'plateaus' and 'valleys' (see figure 1). The surface exhibits two different types of vanadium atoms: coordinatively unsaturated V^t at the top of the 'plateau', linked to another V^t atom via a twofold coordinated oxygen atom $O^t(2)$, and coordinatively saturated V^b lying at the bottom of the 'valley'. Oxygen atoms can be one- or twofold-coordinated, but since the surface is strongly corrugated, they can be placed at the top (t), edge (e) or bottom (b) of the valley. As a result, five distinct oxygen types, denoted $O^t(1)$, $O^t(2)$, $O^e(2)$, $O^b(1)$ and $O^b(2)$, can be distinguished, which exhibit different chemical properties. Especially interesting is the $O^e(2)$ oxygen site that does not appear either at (010) or (100) surfaces, and which originates from the threefold-coordinated oxygen atom in the bulk.

Three slabs containing 4, 6 and 8 layers with 28, 42 and 56 atoms in a supercell, respectively, were used to model the (001) surface. The formation of this surface requires a breaking of strong V–O bonds; hence a pronounced relaxation of the surface should be expected. Surface energies for non-relaxed supercells are equal to 1.15 J m^{-2}, 1.16 J m^{-2} and 1.16 J m^{-2}, respectively. The almost vanishing difference between results obtained for the four-layer and eight-layer slabs indicates that even for the smaller cell the calculations are converged with respect to slab thickness.

Relaxation leads to a dramatic reduction of the surface energy to 0.34 J m^{-2}, 0.44 J m^{-2} and 0.48 J m^{-2}, for four-, six- and eight-layer supercells, respectively. For the supercell containing four layers the relaxation is the strongest, giving the lowest value of surface energy. For thicker slabs, where the bulk-like geometry is preserved in the central layer, the relaxation is less pronounced. The distances between two oxygen atoms ($O^t(2)$ and O placed directly below, see figure 1), may serve as an example. In a four-layer slab this distance increases to 4.42 Å (as compared to 3.57 Å in the bulk) whereas for six- and eight-layer supercells it is stretched to 4.19 Å and 4.09 Å, respectively.

The V–O bond lengths at the (001) surface do not change considerably when the number of layers in the supercell is increased. For all considered slabs the V–O(1) bond length is 1.61 Å, i.e. the same as in the bulk. Bond lengths V^t–$O^t(2)$ and V^t–$O^e(2)$ (on the 'plateau') vary from 1.79 to 1.83 Å. The strongest changes are observed for bonds linking V^b and O(3) lying directly below V^t atoms; they are enlarged by 0.20 Å and 0.08 Å for four- and six-layer slabs, respectively, compared to the corresponding bond lengths calculated for an eight-layer supercell. In contrast, the bonds V^t–O(3) are contracted by 0.12–0.13 Å compared to the bulk for all slabs. Due to the

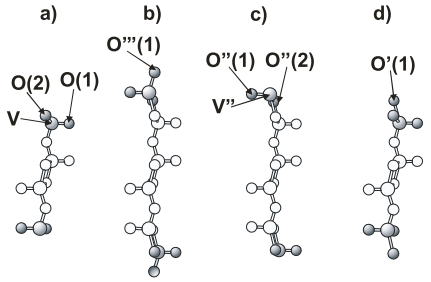

Figure 4. Four possible terminations of the (100) V_2O_5 surface: (a) t_1, (b) t_2, (c) t_3, (d) t_4. The image shows the atomic arrangement in a cell with (1 × 1) surface periodicity.

layer-type character of V_2O_5 some changes in bond lengths appear also in deeper layers, but they never exceed 0.06 Å. It cannot be excluded that the relaxed surface geometry is not completely converged, even for the eight-layer model. However, the remaining uncertainty in the surface energy is very small compared to the difference in the surface energies between (001) and (010) surfaces.

4.3. Geometric structure of the V_2O_5 (100) surface

For the (100) surface four possible terminations exist, out of which only one, denoted as t_1, has a bulk-like stoichiometry (figure 4). Other terminations, denoted as t_2, t_3 and t_4, lead to different compositions of the slab. The (100)-t_1 surface exposes a V atom and two non-equivalent O atoms: O(1) from a vanadyl group with the V–O(1) bond parallel to the surface and twofold-coordinated O(2), which corresponds to the O(3) sites in the bulk. Termination t_4 differs from t_1 by an additional surface oxygen O′(1) bound to the vanadium atom, whereas terminations t_2 and t_3 are derived from t_1 by adding a VO_3 or a VO_2 group, respectively. Different surface oxygen and vanadium sites at (100)-t_3 are denoted as O″(1), O″(2) and V″. The nomenclature used for the surface atoms is defined in figure 4.

Supercells representing terminations t_2, t_3 and t_4 of the (100) V_2O_5 surface (figures 4(b)–(d)) have a non-stoichiometric number of atoms: 22, 20 and 16, respectively. In all cases the supercell has identical surfaces on both sides of the slab. For termination t_1, relaxation does not cause any changes in bond lengths at the surface. The distances between the top V, and O(1) and O(2) are the same as in bulk and equal to 1.61 Å and 1.89 Å, respectively. Small changes in bond lengths appear in deeper layers. The V–O(2) bond (oxygen from the second subsurface layer) is shortened by 0.02 Å and similar changes are found in even deeper layers. For other terminations, changes in geometries are more pronounced (figure 4). The V–O′(1) distance at the (100)-t_4 termination is equal to 1.71 Å (2.05 Å in the bulk), while the similar distance V″–O‴(1) for the (100)-t_2 termination is equal to 1.66 Å (1.79 Å in the bulk). The geometrical changes in the VO_3 (t_2) and VO_2 (t_3) groups (these are the atoms added to the t_1 termination) are strong and vary between 0.05 and 0.39 Å.

The lowest surface energy is calculated for the stoichiometric t_1 termination, 0.61 J m^{-2} for the unrelaxed and 0.55 J m^{-2} for the relaxed surface. The surface energies for other terminations are considerably higher and vary between 0.96 and 4.33 J m^{-2}. However, the relative stabilities of surfaces with different chemical compositions depend also on the chemical potentials of both species. Figures 5(a)–(c) show the plots of surface free energies (calculated according to equation (5)) as a function of $\Delta\mu_O(T, p)$ for all four terminations of the (100) surface at different temperatures and pressures. The upper limit, $\mu_O^{max}(T, p)$, which is the condensation of oxygen on the surface, is taken as a reference and set to 0 eV. The lower limit of the oxygen chemical potential is set by the value where V_2O_5 is reduced to VO_2, $\mu_O^{min}(T, p) = -1.71$ eV. For the entire admissible range of temperatures and oxygen partial pressures the stoichiometric termination (100) V_2O_5-t_1 is the most stable whereas the t_4 is the least stable one. For low chemical potentials (up to about −0.3 eV, corresponding to approximately 1 atm at 298.15 K) the termination t_3 is more stable than t_2, while with increasing pressure the relative stability is reversed.

Table 4. Surface free energies and percentage of low-index V_2O_5 surfaces (for relaxed structures).

	Relaxed	
Surface	E_{surf} (J m^{-2})	Proportion (%)
(010)	0.047	84.5
(001)	0.48	8.3
(100)	0.55	7.2

4.4. Equilibrium morphology of V_2O_5 crystallites

For relaxed geometries, the surface energies for V_2O_5 surfaces are 0.047 J m^{-2}, 0.48 J m^{-2} and 0.55 J m^{-2} for the (010), (001) and (100) surfaces, respectively. The clean (010) surface, having a surface energy that is more than one order of magnitude lower than other surfaces, dominates the crystal morphology determined by the Wulff construction (see figure 6). The estimated percentage of the (010) surface in the total surface area of a V_2O_5 crystallite is 84.5%, while the other two surfaces together contribute the remaining 15.5% (see table 4). The crystal shape derived by the Wulff construction is dominated by the (010) cleavage plane and corresponds to platelets visible in scanning electron microscopy (SEM) [40]. Results of our calculations clearly show that relaxation causes a considerable reduction of the surface energy of the low-index surfaces other than (010), leading to a non-negligible contribution to the total crystallite surface area. Formation of oxygen vacancies on less stable surfaces is expected to be easier compared to saturated (010) surface; therefore these surfaces may play an important role in oxidation catalysis.

5. Electronic structure of (010), (001) and (100) V_2O_5 surfaces

The electronic structure was calculated for the relaxed slabs representing three low-index surfaces. Figures 3(b)–(d) show the partial DOS obtained for the top layers in all cases. None of the three surfaces show a change in the bandwidth, except for

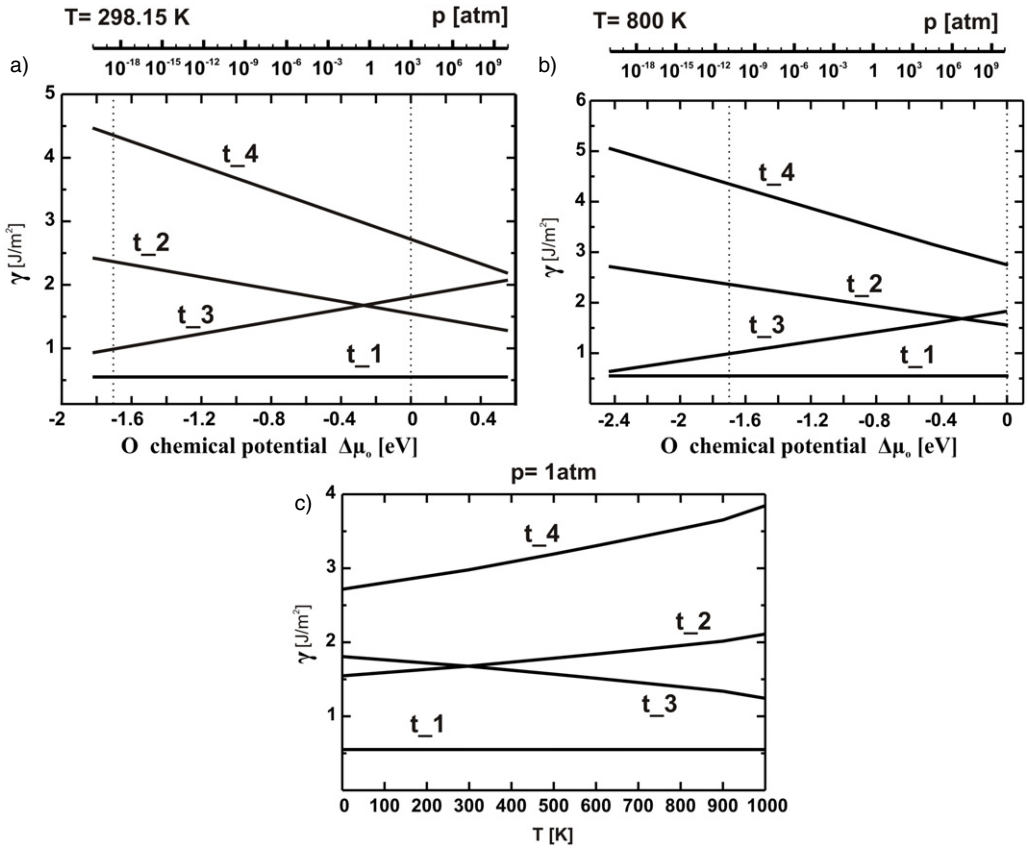

Figure 5. Surface free energies $\gamma(T, p)$ of the four (100) V_2O_5 terminations shown in figure 6 for varying oxygen pressure at constant temperatures $T = 298.15$ K (a), $T = 800$ K (b), and for varying temperature at constant pressure $p = 1$ atm (c).

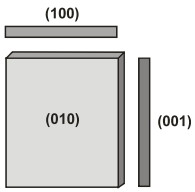

Figure 6. Equilibrium shape of V_2O_5 crystallites resulting from a Wulff construction, showing the areas occupied by the three low-index surfaces.

a slight blurring of the upper edge of the valence band for the least stable (100) surface. The structure of the DOS, however, changes significantly.

The spectrum obtained for a single-layer slab that represents the saturated (010) surface resembles very much the peak structure obtained for the bulk material (compare figures 3(a) and (b)); it consists of a superposition of three peaks: a dominant central and two side peaks. Moreover the maxima of peaks in both spectra are located at similar energies. This indicates weak interaction between layers. In addition the spectrum obtained for (010) V_2O_5 matches experimental UPS data obtained using better resolution for the (010) surface presented in paper [18].

For other two surfaces, calculated densities of states (figures 3(c) and (d)) are much less structured, which is related to the strong structural relaxation of the surface resulting in mixing of the bands derived from the V $3e_g$–O $2p_\sigma$ and V $3t_{2g}$–O $2p_\pi$ interactions. This effect is especially pronounced for the (001) surface where it also causes closing of the narrow gap in the conduction band. For the (100) surface a broadening of the non-bonding O 2p band at the top of the valence band, leading to a blurring of the VB edge, is observed. Unfortunately, no experimental results are available for these surfaces.

6. Summary

First-principles DFT calculations were used to study the atomic and electronic structure of bulk V_2O_5 and of its three low-index surfaces: (010), (001) and (100). The bulk geometry optimized at the GGA level is in good agreement with experimental results. Also the widths of valence bands and the gap widths match very well experimental data. Strong hybridization between the O 2p and V 3d states determines the shape of the valence band, whereas the conduction band consists mainly of V 3d orbitals. Interaction between bulk V_2O_5 layers is found to be weak. This is reflected by a close similarity between the DOS of the bulk and a single-layer slab representing the (010) surface. For the (001) surface a strong relaxation effect is observed, resulting in a decrease of surface energy by a factor of about 2.4 as compared to 1.15 for (010) and 1.11 for (100). For the (100) surface the stability of four different terminations in equilibrium with the oxygen environment is analysed. The t_1 stoichiometric termination is found to be the

most stable, while the other non-stoichiometric terminations are energetically disfavoured. The calculated surface free energies for the (010) surface are one order of magnitude lower than those for (100) and (001). Correspondingly, the (010) surface dominates in a Wulff construction of the equilibrium crystal shape of V_2O_5. The high stability of the (010) surface is largely connected to its coordinatively saturated geometric structure. The obtained Wulff polyhedron shows a close resemblance to the equilibrium shape of real V_2O_5 obtained by the SEM technique. Because of the very low amount of the experimental information about unsaturated low-indices V_2O_5 surfaces, the qualitative discussion is possible only for the (010) V_2O_5 face. However, even if the (100) and (001) V_2O_5 surfaces constitute only 15.5% of the total surface area in Wulff's polyhedron, they cannot be *a priori* excluded and may play important role in the catalytic processes.

Acknowledgments

The Kraków-Wien cooperation has been supported by a Marie-Curie fellowship of JG at the Marie-Curie Training Site 'Atomic Scale Computational Materials Science' at the Universität Wien. Work in Wien has also been supported by the Austrian Science Funds under project no. P19983-N16. The authors acknowledge financial support of the Polish Ministry of Sciences (grant N204 024 31/0475).

References

[1] Grzybowska-Świerkosz B 2002 *Top. Catal.* **21** 35
[2] Cavani F and Trifiro F 1997 *Catal. Today* **36** 431
[3] Centi G, Cavani F and Trifiro F 2001 *Selective Oxidation by Heterogeneous Catalysis* (New York: Kluwer Academic)
[4] Mars P and van Krevelen D W 1954 *Spec. Suppl. Chem. Eng. Sci.* **3** 41
[5] Witko M 1996 *Catal. Today* **32** 89
[6] Hermann K, Witko M, Druzinic R and Tokarz R 2000 *Top. Catal.* **11/12** 67
[7] Tokarz-Sobieraj R, Witko M and Gryboś R 2005 *Catal. Today* **99** 241
[8] Haber J and Witko M 2003 *J. Catal.* **216** 416
[9] Chakrabarti A, Hermann K, Druzinic R, Witko M, Wagner F and Petersen M 1999 *Phys. Rev.* B **59** 10583
[10] Kresse G, Surnev S, Ramsey M G and Netzer F P 2001 *Surf. Sci.* **492** 329
[11] Ganduglia-Pirovano M V and Sauer J 2004 *Phys. Rev.* B **70** 045422
[12] Brazdova V, Ganduglia-Pirovano M and Sauer J 2004 *Phys. Rev.* B **69** 165420
[13] Oshio T, Sakai Y, Moriya T and Ehara S 1993 *Scanning Microsc.* **7** 33
[14] Oshio T, Sakai Y and Ehara S 1994 *J. Vac. Sci. Technol.* B **12** 2055
[15] Smith R L, Lu W and Rohrer G S 1995 *Surf. Sci.* **322** 293
[16] Smith R L, Rohrer G S, Lee K S, Seo D-K and Whangbo M-K 1996 *Surf. Sci.* **367** 87
[17] Da Costa A, Mathieu Ch, Barbaux Y, Poelman H, Dalmai-Vennik G and Fiermans L 1997 *Surf. Sci.* **370** 339
[18] Hermann K, Witko M, Druzinic R, Chakrabarti A, Tepper B, Elsner M, Gorschlüter A, Kuhlenbeck H and Freund H-J 1999 *J. Electron. Spectrosc. Relat. Phenom.* **98/99** 245
[19] Kresse G and Joubert D 1999 *Phys. Rev.* B **59** 1758
[20] Perdew J P and Wang Y 1992 *Phys. Rev.* B **45** 13244
[21] Blöchl P E 1994 *Phys. Rev.* B **50** 17953
[22] Monkhorst H J and Pack J D 1976 *Phys. Rev.* B **13** 5188
[23] Reuter K and Scheffler M 2001 *Phys. Rev.* B **65** 035406
[24] Wulff G 1901 *Z. Kristallogr.* **34** 449
[25] Enjalbert R and Galy J 1986 *Acta Crystallogr.* C **42** 1467
[26] Bachmann H G, Ahmed F R and Barnes W H 1961 *Z. Kristallogr.* **115** 110
[27] Murnaghan F D 1944 *Proc. Natl Acad. Sci. USA* **30** 244
[28] Rydberg H, Dion M, Jacobson N, Schröder E, Hyldgaard P, Simak S I, Langreth D C and Lundqvist B I 2003 *Phys. Rev. Lett.* **91** 126402
[29] Lein M, Dobson J F and Gross E K U 1999 *J. Comput. Chem.* **20** 12
[30] Van Hieu N and Lichtman D 1980 *J. Vac. Sci. Technol.* **18** 49 and references therein
[31] Cogan S F, Nyugen N M, Perrotti S J and Rauh R D 1989 *J. Appl. Phys.* **66** 1333
[32] Moshfegh A Z and Ignatiev A 1991 *Thin Solid Films* **198** 251
[33] Eyert V and Hőck K-H 1998 *Phys. Rev.* B **57** 12727
[34] Lambrecht W, Djafari-Rouhani B, Lannoo M and Vennik J 1980 *J. Phys. C: Solid State Phys.* **13** 2485
[35] Shin S, Suga S, Taniguchi M, Fujisawa M, Kanzaki H, Fujimori A, Daimon H, Ueda Y, Kosuge K and Kachi S 1990 *Phys. Rev.* B **41** 4993
[36] Yeh J and Lindau I 1985 *At. Data Nucl. Data Tables* **39** 1
[37] Wu Q H, Thissen A, Jaegermann W, Schütz M and Schmidt P C 2006 *Chem. Phys. Lett.* **430** 309
[38] Laubach S, Schmidt P C, Thißen A, Fernandez-Madrigal F J, Wu Q-H, Jaegermann W, Klemm M and Horn S 2007 *Phys. Chem. Chem. Phys.* **20** 2564
[39] Khyzhun O Yu, Strunkus T, Grünert W and Wöll Ch 2005 *J. Electron. Spectrosc. Relat. Phenom.* **149** 45
[40] Ozkan U S, Cai Y and Kumthekar M W 1993 *Appl. Catal.* A **96** 365